Received: 3 August 2021 | Revised: 17 January 2022 | Accepted: 23 January 2022

DOI: 10.1002/esp.5358

RESEARCH ARTICLE

ESPL WILEY

Disproportionate and chronic sediment delivery from a fluvially controlled, deep-seated landslide in Aotearoa New Zealand

Samuel Thomas McColl[1,2] | Charlotte Naomi Holdsworth[3] | Ian Christopher Fuller[1] | Malcolm Todd[4] | Forrest Williams[1]

[1]School of Agriculture and Environment, Massey University, Palmerston North, New Zealand

[2]GNS Science, Lower Hutt, New Zealand

[3]John Turkington Limited, Marton, New Zealand

[4]Horizons Regional Council, Palmerston North, New Zealand

Correspondence
Samuel Thomas McColl, GNS Science, 1 Fairway Drive, Avalon, Lower Hutt 5011, New Zealand.
Email: s.mccoll@gns.cri.nz

Funding information
British Socieity for Geomorphology Research Grant; New Zealand Ministry of Business, Innovation and Employment research program 'Smarter Targeting of Erosion Control (STEC)' (Contract C09X1804); Eric Ojala Sub-Trust Grant; Canon Environmental Grant

Abstract

Past research has highlighted the importance of sediment delivery from multiple-occurrence regional landslide events triggered by storms or earthquakes. Herein, we examine delivery from a more persistent source of sediment, that of a large, slow-moving landslide in the soft-rock hill country of Aotearoa New Zealand. We map and monitor the 80-ha Rangitikei Landslide from 2015 to 2019 using time-lapse photography, ground surveys, photogrammetry, and piezometers. We show that the landslide can be divided into several zones with distinctive movement patterns, but all zones respond to river erosion. The fastest zone moves more than 10 m per year in a flow-like fashion, while other zones move 0.01 m per year via slow sliding. Movement occurs all year round, but is two to three times faster in winter and spring. While rainfall and associated groundwater change are commonly attributed to landslide movement patterns, our data show that river flow correlates closely with the weekly to seasonal variability in movement of the landslide toe. This suggests that fluvial erosion can play an important role in the movement dynamics of highly coupled landslides. We estimate an annual sediment yield to the Rangitikei River of at least 40 000 tonnes, in this first quantification of sediment delivery from an active soft-rock landslide in Aotearoa. This volume implies 7% of the total catchment suspended sediment yield is derived from 0.03% of the contributing catchment area, demonstrating the disproportionate effect of this (and likely other) deep-seated landslide(s) as a source of sediment in the Rangitikei catchment. Sediment delivery is more continuous than the episodic supply of multiple-occurrence regional landslide triggering events, and by delivering mostly fine-grained sediment, it has a potentially large impact on water quality.

KEYWORDS
fluvial incision, hillslope erosion, landslide monitoring, mass movement, sediment yield, slope–channel coupling

1 | INTRODUCTION

Landslides are a dominant process of hillslope erosion (e.g. Arsenault & Meigs, 2005; Korup et al., 2007; Mackey & Roering, 2011), landscape evolution (Booth et al., 2013; Korup, 2008; Larsen et al., 2010), and sediment and solute generation (e.g. Emberson et al., 2016; Korup, 2005; Korup et al., 2004). Their geomorphic work is most vividly apparent during extreme triggering events, which can induce tens of thousands of landslides almost instantaneously across a landscape, causing a major pulse of erosion and sediment delivery (Crozier, 2005). For example, the ~62 000 landslides and many millions of cubic metres of erosion generated by the 2004 Manawatū storm event in Aotearoa New Zealand (Dymond et al., 2006), or the sustained sediment loading of rivers from the landslides generated by the 1999 Chi-Chi earthquake

and subsequent storm events in Taiwan (Lin et al., 2008). In contrast, while less dramatic agents of geomorphic change, the potential longevity (i.e. millennia) and large size (i.e. >10 000 m^2) of slow-moving bedrock landslides can mean these individual features produce a significant long-term impact (Basher et al., 2018; Mackey & Roering, 2011; Nereson & Finnegan, 2018). The continuous movement of soft-bedrock landslides can reshape entire hillslopes. Their common coupling to a river network makes such mass movements a chronic but major contributor to landscape evolution and long-term sediment flux, and a damaging, albeit seldom life-threatening, hazard (Mackey & Roering, 2011; Massey et al., 2013; McColl & McCabe, 2016; Simoni et al., 2013).

Many mass movements share a close relationship with the fluvial network. Fluvial incision or bank erosion destabilizes hillslopes, and in areas of intense fluvial incision landslide erosion prevails (Larsen & Montgomery, 2012). Delivery of clastic landslide sediments can influence river form and process, by enhancing erosion or forcing channel adjustments (or blockages) and through bed armouring (Bennett et al., 2016a; Egholm et al., 2013; Korup, 2006). This fluvial interaction depends on the nature of the landslide sediment, hillslope–channel coupling, and rate of delivery. For multiple-occurrence regional landslide events, usually only some proportion of all landslides are connected to the river; for example, approximately 8% of landslides connected to rivers in the 1999 Chi-Chi earthquake in Taiwan, with 13 and 24% connected in the following Typhoon Toraji and Herb, respectively (Dadson et al., 2004); 67% of landslides were connected in the 2004 Manawatū storm (Hancox & Wright, 2005). In comparison, many chronic (long-lived, slow-moving) landslides exist because of, or are sustained by, river incision and therefore are directly coupled to the river network (Bilderback et al., 2014; Mackey & Roering, 2011; Nereson & Finnegan, 2018). Such situations may be common in rapidly uplifting and incising landscapes where hillslopes exist at threshold slope angles (Larsen & Montgomery, 2012), or in landscapes in which geological structures render slopes sensitive to fluvial dissection (Williams et al., 2021).

Due to the often strong coupling of long-lived, slow-moving landslides to river systems, they are an important, but seldom quantified, long-term source of sediment delivery to rivers. In particular, to date there has been little quantification of the contemporary delivery of sediment from such landslides (cf. Bilderback et al., 2014), or exploration of how these delivery rates change over sub-annual timescales (cf. Bovis & Jones, 1992). Furthermore, investigation of the causes of sub-annual movement variability and the dynamic relationships between fluvial incision and movement over sub-annual timescales, relative to other mass-movement drivers (e.g. rainfall), has seldom been explored. Herein, we help to address this shortcoming by examining the movement and sediment delivery of the deep-seated Rangitikei Landslide in the North Island of Aotearoa New Zealand. The landslide occurs within Neogene marine sedimentary rocks, which cover about 17% of Aotearoa, and about 30% of the North Island (Edbrooke et al., 2015). The weak nature of these rocks renders the landscapes highly prone to slope instability, even at low hillslope gradient, and the spatial persistence of bedding planes permits very sizeable landslides to develop, some of which exceed multiple square kilometres in area (Williams et al., 2021). Over 7000 landslides (>2 ha), including the Rangitikei Landslide, have been mapped within Aotearoa's Neogene cover rocks (Massey et al., 2016; Rosser et al., 2017). While some of these mapped landslides are likely discrete failure events that experienced a single or short-lived period of motion (e.g. earthquake triggered; Crozier & Pillans, 1991; Massey et al., 2018b; Mountjoy & Pettinga, 2006), many are likely to be long lived (>100 years old). Some dated landslides in Aotearoa are many thousands of years old (e.g. Beetham et al., 2002; Bilderback et al., 2014) and remain active or dormant, similar to long-lived landslides found elsewhere in the world (e.g. Bovis & Jones, 1992; Nereson et al., 2018). Such landslides continuously or episodically move and deliver sediment to the river network (Massey et al., 2013, 2018a). The fine-grained nature of these weak materials results in the almost instantaneous production of suspended sediment upon entering the river network, creating potential water quality and ecological health implications (Ballantine et al., 2015; Davies-Colley, 2013). Quantification of the delivery of fine sediment from slow-moving landslides and its variability compared with other sediment sources (e.g. shallow, soil-stripping landslides or bank erosion) is needed to inform land management and suitable national policy targets for sediment reduction strategies.

2 | STUDY AREA

2.1 | Geology and geomorphology

Rangitikei Landslide is within hill-country terrain cut into the Neogene marine sedimentary cover rocks of the Whanganui Basin, central North Island, Aotearoa (Figure 1; landslide centroid = 175.854°E, 39.751°S). The rocks are predominantly weak (<1–20 MPa unconfined compressive strength) mudstones, sandstones, and siltstones, with occasional stronger calcareous or concretionary layers, and very weak clay seams (Lee et al., 2011; Massey et al., 2018a; Rees et al., 2020) (Figure 1). The cover rocks rest upon the much stronger (UCS > ~150 MPa) basement Torlesse greywacke rocks, which outcrop to the east where erosion from uplift of the axial ranges has exposed them (Lee et al., 2011). West of the axial ranges, the preservation of the cover rocks, and the persistence of planar to gently deformed bedding layers, reflects the lower rates of uplift, but tectonic activity has regionally and locally tilted, folded, and faulted the rocks. The regional dip/inclination of the bedding is 3–7° to the south–southwest (Massey, 2010), but faulting and folding cause local variation. The cover rocks have been strongly dissected by fluvial incision, with suites of Pleistocene–Holocene strath terraces and deeply incised river valleys (Litchfield & Berryman, 2006; Milne, 1973; Rees et al., 2020). Mostly greywacke river gravels and sands cap the river terraces, which in places are preserved as flat terraces, and in other places are deformed and reworked by mass-movement processes. The fluvial incision, in combination with spatially persistent, dipping clay layers, gives rise to hillslope instability and the formation of numerous large, translational landslides in the cover rocks, along with rotational landslides and earthflows (Williams et al., 2021).

2.2 | Poroa Landslide Complex

Rangitikei Landslide is part of the (c. 11 km^2) Poroa Landslide Complex (Thomson, 1982). The Poroa Landslide Complex is bounded to the west by the Hautapu River and to the south by the Rangitikei

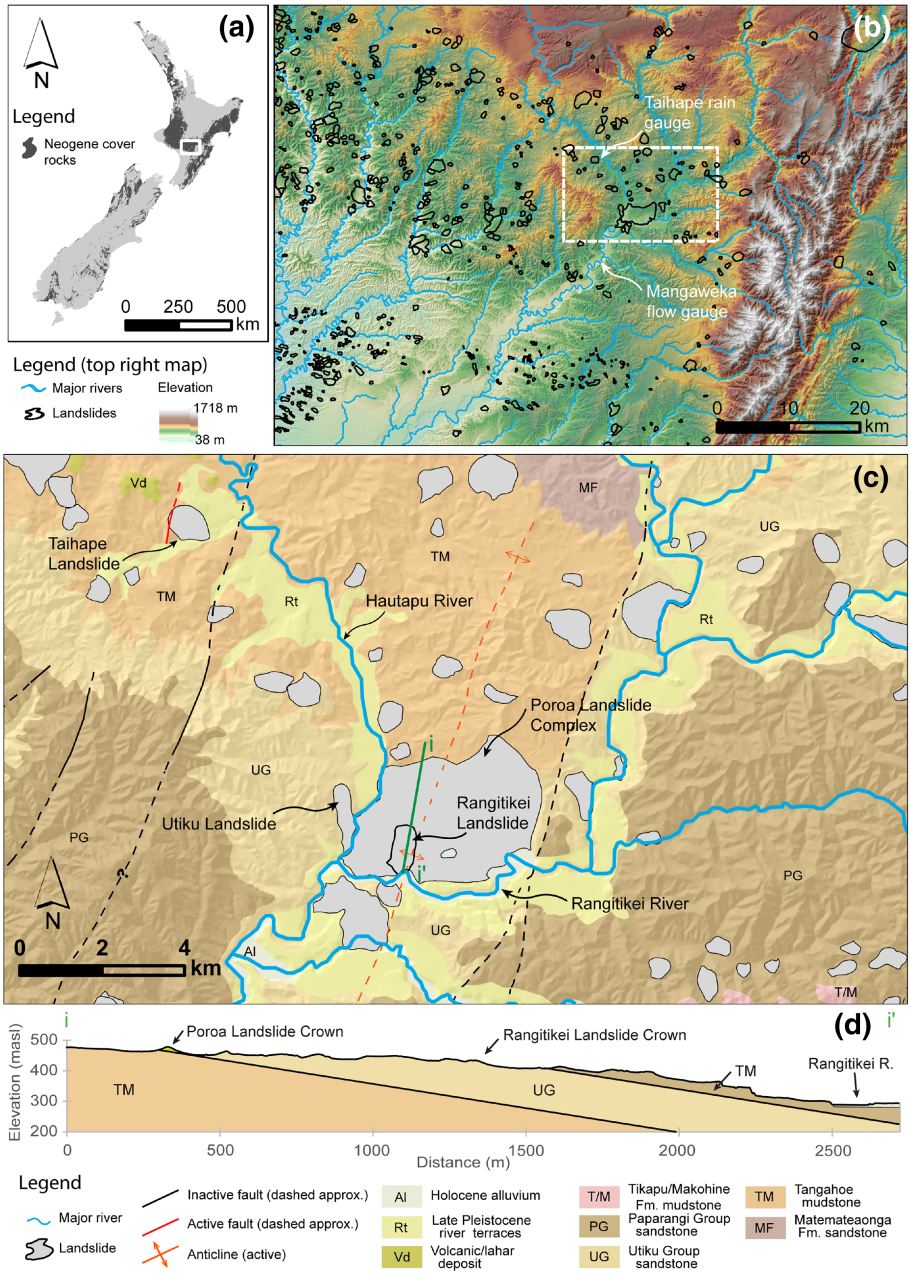

FIGURE 1 Location of the Rangitikei Landslide and geological setting. (a) Location of map b in the North Island of Aotearoa, with dark grey shading showing the distribution of Neogene sedimentary cover rocks from Edbrooke et al. (2015). (b) 25 m coloured digital elevation and transparent hillshade model and major river network (from land information New Zealand, LINZ). Black polygons represent the GNS Science large landslide database (Rosser et al., 2017) and mapping by Williams et al. (2021). The Taihape rain gauge and Mangaweka flow gauge are labelled. The extent of map c is marked by the white dashed rectangle. (c) Geology surrounding the Rangitikei Landslide showing the cover rocks, faults and folds, along with major landslide outlines. (d) Schematic (approximate) geological cross-section through Poroa Landslide Complex at position (i–i') marked on map c. Geological data for panels c and d are simplified from Lee et al. (2011) and Townsend et al. (2008) [Color figure can be viewed at wileyonlinelibrary.com]

River, extending about 5 km eastwards along the Rangitikei River (Figures 1 and 2). Failure of the complex likely involves translational/planar sliding along gently inclined weak sedimentary strata (e.g. clay layers), similar to other deep-seated landslides in the area (e.g. the neighbouring Utiku Landslide; Massey et al., 2013). While no data are available on bedding attitudes in the landslide, bedding sighted on the opposite side of the Rangitikei River from the Rangitikei Landslide has an apparent dip of a few degrees towards the west (true dip likely SSW). This is consistent with the mapped position of an anticline that transects the Poroa Landslide Complex just east of Rangitikei Landslide (Figure 1), and a dip direction of ~230° from three-point solution of borehole data for the failure surface of the adjacent Utiku Landslide (~1 km to the west) (Massey, 2010). The depth of the complex is unknown, but given its areal extent it is likely many tens to hundreds of metres thick and displacing Tangahoe Mudstone Formation (Taihape Group) and Tarare Formation (Utiku Group) rocks. The complex is compartmentalized into several smaller landslides, with movement directions that differ due to variance in the local bedding inclination, resulting from a SSW–NNE-trending anticline that passes through the middle of the landslide complex (Lee et al., 2011) and river valleys on multiple sides (Figure 2b).

2.3 | The Rangitikei Landslide

The 0.80 km^2 Rangitikei Landslide is a discrete mass movement of the Poroa complex (Figure 2), first mapped and described by Thomson (1982). The landslide is bounded on either side by lateral shears (strike-slip 'faults') or drainage lines, suggesting that it moves partly independently of the other parts of the complex (Figure 2c). The upslope boundary is deemed to be a head graben (i.e. zone of subsidence driven by extensional displacements within landslides), which hosts a lake/wetland named John's Swamp (Figure 2). The toe of the landslide is trimmed by the Rangitikei River. In the current river alignment, the landslide toe forms an outside bend of the river, with river flow directed into the landslide toe (Figure 2e). The landslide is

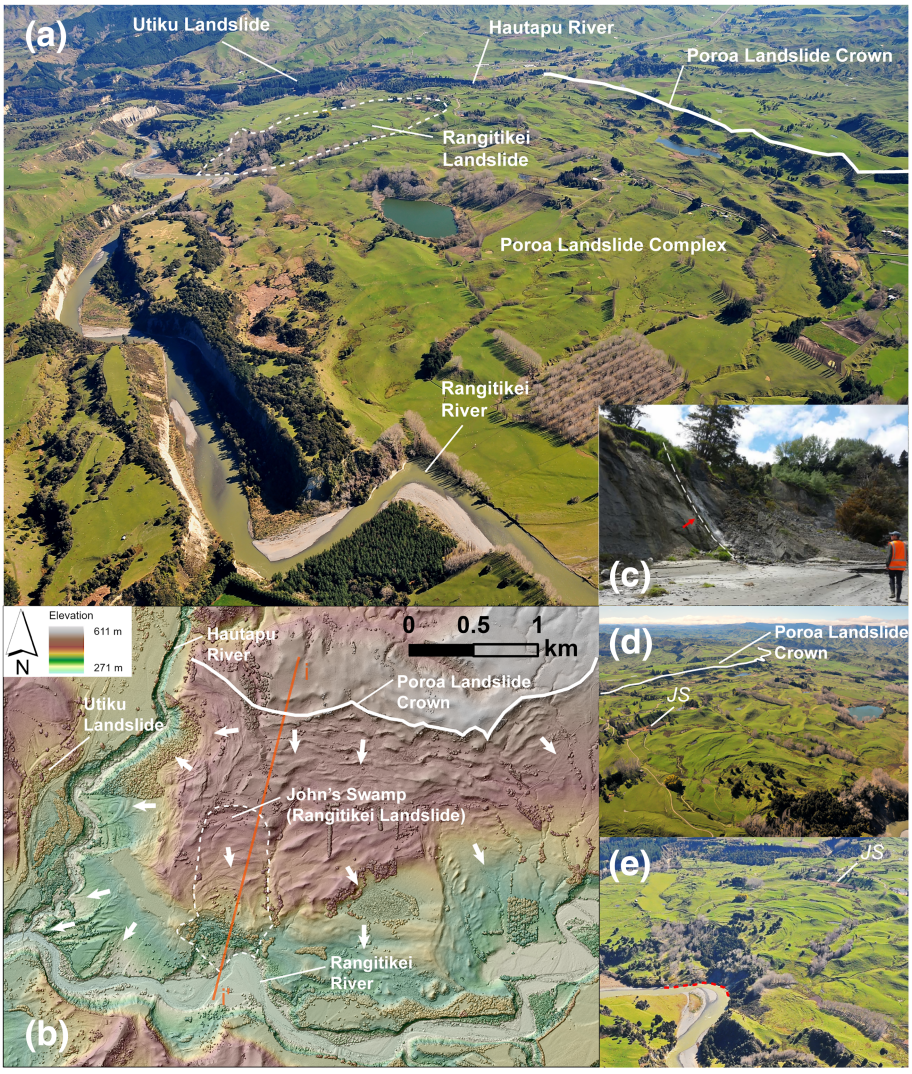

FIGURE 2 (a) Poroa Landslide Complex and the Rangitikei Landslide (white dashed outline), looking west. (b) Coloured hillshade model of Poroa Landslide Complex, based on 1 m digital surface model courtesy of Horizons Regional Council. (c) The true right boundary of the Rangitikei Landslide at the landslide toe indicated by the white dashed line and red arrow. (d) View of Poroa Landslide with Rangitikei Landslide in foreground, looking northeast (JS = John's Swamp). (e) View of Rangitikei Landslide looking northwest with Rangitikei River flowing into the toe of the landslide (red dashed arc) and the stand of trees in the lower section of the landslide. Photos in a, d, and e taken in August 2009 by Graham Hancox. Photo in c taken by C. Holdsworth [Color figure can be viewed at wileyonlinelibrary.com]

part of a working sheep and beef farm, with pasture giving way to a stand of native and exotic trees in the lower part of the landslide. Farm tracks, fences, and small buildings have experienced damage from landslide movement. The landslide is reported by the farmer to have undergone phases (i.e. years to decades) of more rapid movement, similar to what has been observed for other landslides in the Neogene cover rocks in the lower North Island (Massey et al., 2016; McColl & McCabe, 2016). In 2015 the landslide was reported to have begun another phase of more rapid displacement that continues to the present day, prompting the current investigation.

3 | METHODS

3.1 | Survey network

To monitor landslide movement, 30 survey pegs (0.5 m steel stakes) were distributed on and around the landslide (Figure 3). Some were placed outside of the assumed landslide boundary to provide a means of confirming the landslide boundary delineation within the Poroa Landslide Complex. The positions of all pegs were measured using Trimble R10 and R8 GNSS receivers in real-time kinematic (RTK) or post-processed kinematic (PPK) survey mode at 3–6 monthly intervals between July 2015 and October 2019. A Land and Survey New Zealand (LINZ) benchmark (B47B) on Carlson Road, Utiku was used as a fixed reference (i.e. base station control point) for all surveys, with a maximum differential correction baseline of less than 2.5 km. It is assumed that B47B is stable (other than regional tectonic deformation), and that any movement measured at the study site, above the detection threshold, is recording real ground movement (where disturbance by stock animals can be discounted). Trimble Business Centre 5.0 was used for differential GNSS processing, with most resulting precisions (as reported by Trimble Business Centre) below 0.06 m horizontally (max = 0.058, mean = 0.039, standard deviation [s.d.] = 0.013 m) and 0.1 m vertically (max = 0.086, mean = 0.056, s.d. = 0.018 m); few observations exceeded 0.1 m precisions and those were removed from the analyses. Repeat occupations of one or more survey pegs during each survey (to evaluate intra-survey accuracy) were within 0.035 m horizontally of each other (max = 0.034, mean = 0.012, s.d. = 0.009 m) and 0.015 m vertically (max = 0.013 m, mean = 0.007, s.d. = 0.003 m). Occupations of the same 'stable' peg (peg 1; Figure 3a) outside of the inferred landslide boundary between subsequent surveys (to evaluate inter-survey accuracy) were all within 0.065 m horizontally of each other (max = 0.064, mean = 0.027, s.d. = 0.014) and 0.19 m vertically (max = 0.184, mean = 0.050, s.d. = 0.057 m). All positions were recorded as grid coordinates in NZGD 2000 NZTM and elevations are relative to the New Zealand 2016 Vertical Datum (NZVD2016).

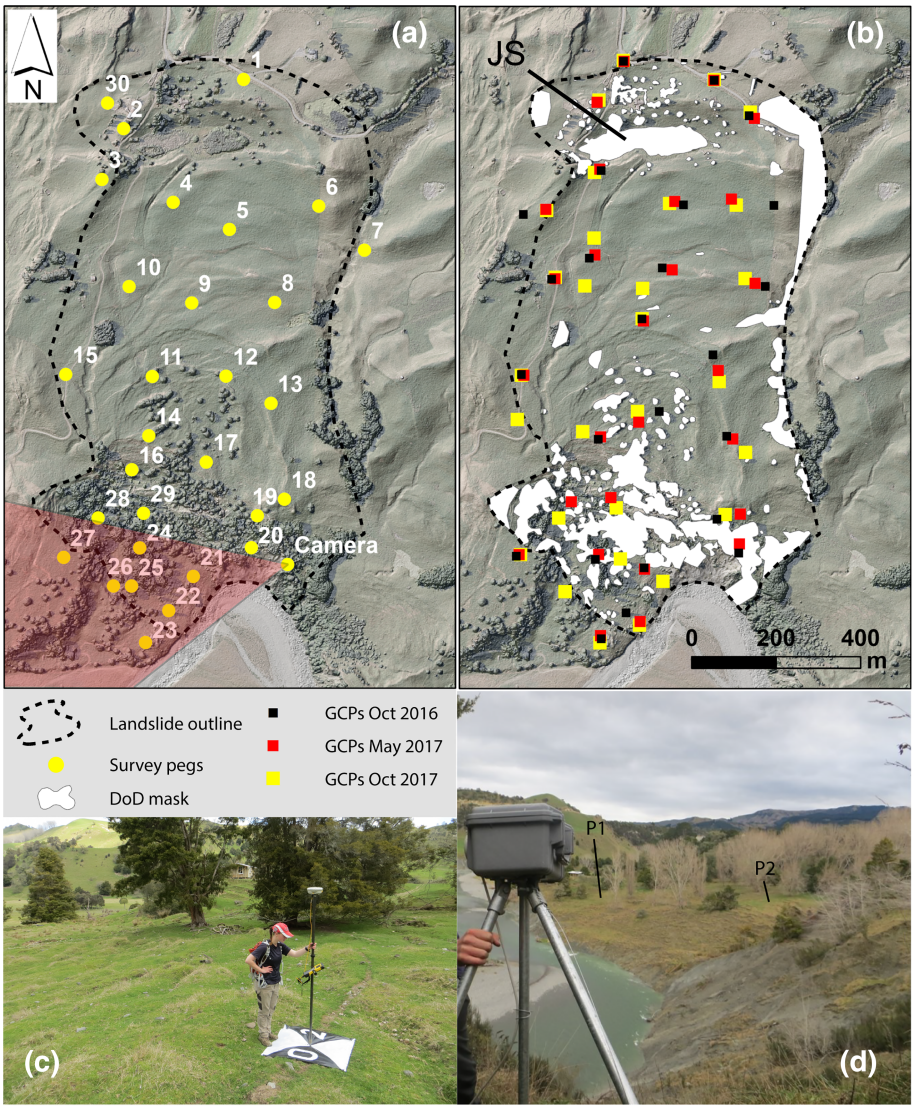

FIGURE 3 (a) Location of survey pegs on and around Rangitikei Landslide, and location of time-lapse camera with approximate field of view shown by the pink shaded area. (b) Ground control point distributions for SfM photogrammetry surveys and example of masking of vegetation, water features, and other excluded areas in the DEM differencing (October 2016–May 2017). JS = John's Swamp. (c) Example of ground control target being surveyed with R8 RTK GPS. (d) Time-lapse camera and approximate field of view across the toe and lower zones of the landslide and with Rangitikei River (looking downstream). P1 and P2 mark the locations of the two piezometers. The imagery in a and b is 2016 0.3 m aerial photography provided by Land Information New Zealand with an associated transparent hillshade model based on 1 m digital surface model courtesy of Horizons Regional Council [Color figure can be viewed at wileyonlinelibrary.com]

3.2 | Geomorphological mapping and morphological change assessment

High-resolution (50 cm) digital elevation models (DEMs) and (5 cm) orthophoto mosaics were produced for the purposes of geomorphic change assessment and geomorphological mapping. These data were produced using Structure-from-Motion (SfM) photogrammetry from aerial photography surveys in October 2016, May 2017, and October 2017. Aerial photos were collected using a Phantom 3 Professional remotely piloted aircraft (RPA) with a 20 mm (35 mm format equivalent) lens and 12-megapixel sensor. For each survey a systematic flight pattern was flown with an above-ground elevation of 50–60 m, and nadir (vertical) camera orientation to achieve a minimum of 75% forward and 65% side overlap between photos. Each flight path was flown a second time with an oblique (~30° from nadir) camera orientation to maximize photo overlap and help reduce radial distortion common to SfM photogrammetry (as shown by James & Robson, 2014). Prior to each collection, 24–28 ground control points (GCPs), consisting of 1 m-square plastic sheets, were distributed around the margins of and within the main body of the landslide (Figure 3b). Their centroids were surveyed with RTK GNSS to provide georeferencing and lens calibration for the photogrammetry models. The horizontal and vertical GNSS precisions reported by Trimble Business Centre were used for defining the GCP uncertainties in the photogrammetry software, but with additional allowances of 0.01 m horizontal and 0.02 m vertical error for survey pole tip placement on the GCP centres. Agisoft Metashape 1.6.2 was used for SfM photogrammetry processing, with the key processing parameters and steps used presented in Supplementary Table S1. DEMs, produced following point cloud classification and manual editing to remove trees, were imported into ArcMap 10.6. To evaluate DEM accuracy, the survey pegs were used as independent check points. The number of check points used in each survey varied between 14 and 22, depending on peg visibility within the resulting orthophoto mosaics. The elevation difference between each check point collected in the field and the respective DEM was calculated, along with the mean, root mean square error (RMSE), maximum, and minimum of the values (Table S1).

To assess changes in landslide morphology and to quantify volumetric changes (i.e. erosion and sediment export), the DEMs were differenced using the Geomorphic Change Detection (GCD) tool (Wheaton, 2015) in ArcMap. Three DEMs of difference (DoDs) were produced to compare change across 1 year (October 2016–October 2017) and within the year to compare summer (October 2016–May 2017) and winter (May 2017–October 2017) change for the entire landslide. After reviewing the results, which presented little detectable change in the upper landslide zones, three new DoDs were produced

for the same epochs, but for the lower (more active) zones of the landslide only. The lower zones of the landslide experience the greatest movement and are better captured by the distribution of GCPs, allowing more reliable detection of change and volumetric change calculations. The RMSE value from the independent check points was used to produce a uniform error surface for each DEM, which were then propagated, using standard error propagation (equation [2] of Wheaton et al., 2010) and used as a minimum level of detection (mLoD) for the DoD (Wheaton, 2015). Although point cloud classification and editing were applied to remove trees in the DEM generation, due to uncertainty of DEM interpolation within heavily treed areas, areas of tree cover (and water bodies) were delineated and applied as masks in GCD to exclude these from the DEM differencing (Figure 3). Masking was done separately for each DEM (due to changes in the positions of objects from landslide movement) and used to produce a unique area of interest (i.e. analysis area) for each DoD. This helped to provide more reliable DoDs free from areas of unreliable (i.e. non-ground) data, but it results in a slightly different area of analysis for each DoD.

The DEM hillshades and orthophoto mosaics, along with field inspection, were used to characterize the geomorphology of the landslide. The types and distribution of mass movement strain indicators (e.g. scarps, anti-scarps, shear zones, and other ground damage) were noted, along with overall slope morphology. This, in combination with the survey peg data and DoD, allowed the partitioning of the landslide into zones with distinct geomorphology or landslide characteristics.

3.3 | Time-lapse photography

A camera was installed in July 2015, looking across the lower landslide, to track movement at the toe of the landslide where movement was assumed to be greatest (based on anecdotal information and morphological observations) and to monitor the relationships between fluvial erosion and landslide movement patterns (Figure 3). The camera was controlled using a custom-built timer and a Raspberry Pi computer board to capture hourly photos during daylight hours. The camera was a Canon 700D SLR with a 24 mm fixed focal length lens with focus set at infinity, housed in a waterproof casing, and powered with a 12 V battery and solar panel. Time-lapse videos were made by selecting one photo per day, targeted at 11 am unless visibility was better earlier or later in the day. Time-lapse videos permit the pattern of movement to be visualized. Weekly images were also selected for quantitative movement measurement using pixel tracking, with the software Point Catcher v2.0 (www.lancaster.ac.uk/staff/jamesm/software/pointcatcher.htm) (James et al., 2016). The time-lapse camera was considered to be located in a stable position beyond the main landslide boundary, relatively free from movement during the course of the study. This was confirmed by GPS monitoring of a survey peg at the camera, and reviewing changes in the camera field of view. Consequently, time-lapse images were not registered to remove camera movement (deemed negligible relative to the real movement observed). For some of the analyses presented, the data were georeferenced using a DEM from the SfM processing, while for some analyses they are not georeferenced. Georeferencing provides a means of extracting real-world coordinates or object movement in units of metres, but DEM fitting introduces error and since the purpose was mainly to assess the timing of movement rather than absolute distances, movement in units of pixel displacement was considered adequate.

3.4 | Piezometric monitoring and hydrological data

In October 2017 two standpipe piezometers (P1 and P2) were installed in the lower part of the landslide (Figure 3d), to assess the relationship between rainfall, groundwater levels (porewater pressure), and movement within the lowermost (fastest moving) zone of the landslide. The piezometers (PVC pipe with screened section near the base) were installed into holes excavated by a percussion corer. The depth of each hole was targeted at an inferred failure surface of the earthflow slide in that location. The failure surface depth was approximated by projecting its position into the slope from an exposure of the failure surface in the riverbank at the landslide toe (Figure 2c). The failure surface was assumed to be met when the corer reached a relatively impenetrable layer, compared to the broken, soft ground of the remoulded earthflow material. P1 was installed on the western side of the landslide to a depth of 2.5 m. P2 was installed about 100 m east, on higher ground, to a depth of 11 m. Solinst (levelogger) digital water-level loggers were set at the base of each piezometer (i.e. just above the assumed failure surface), with a recording interval of 5 min. A barometer was positioned on a nearby building at a similar elevation to allow air pressure variations to be compensated for. While the holes were not manually backfilled or sealed, the holes quickly collapsed around the pipes and are assumed to have provided a suitable natural seal due to the soft, clay-rich nature of the landslide material. For comparison of landslide movement rates against rainfall and river flow, we used nearby Horizons Regional Council monitoring stations (Figure 1b). Mean daily flow on the Rangitikei River was taken from a flow gauge at Mangaweka, approximately 8 km downstream; while it captures additional flow from several tributaries downstream of the landslide, the catchment area upstream of the landslide is larger. Daily rainfall totals were taken from a rain gauge at Taihape, approximately 10 km NNW in similar terrain to the Rangitikei Landslide.

4 | RESULTS

4.1 | Landslide morphological zonation

Identification of ground damage, morphology, and structural features has permitted the discretization of the Rangitikei Landslide into zones with distinct stress regimes and geomorphology; planar sliding, transitional, earthflow-sliding, and passive zones (Figure 4). The planar sliding zone (PSZ) occupies the upper half of the landslide and is characterized by gently sloping ground (~3–4°, but locally steeper) dissected by grabens with opposing 'normal fault' scarps (Figures 4b and g). The grabens and scarps extend across the whole width of the landslide and strike approximately ENE, sub-parallel (i.e. slightly oblique) to the slope contours. While the grabens themselves undergo subsidence, this and their presence is assumed to be in response to extension resulting from sliding along a planar failure surface (Figure 5). Two zones (TZ1 and TZ2) in the central to lower third of

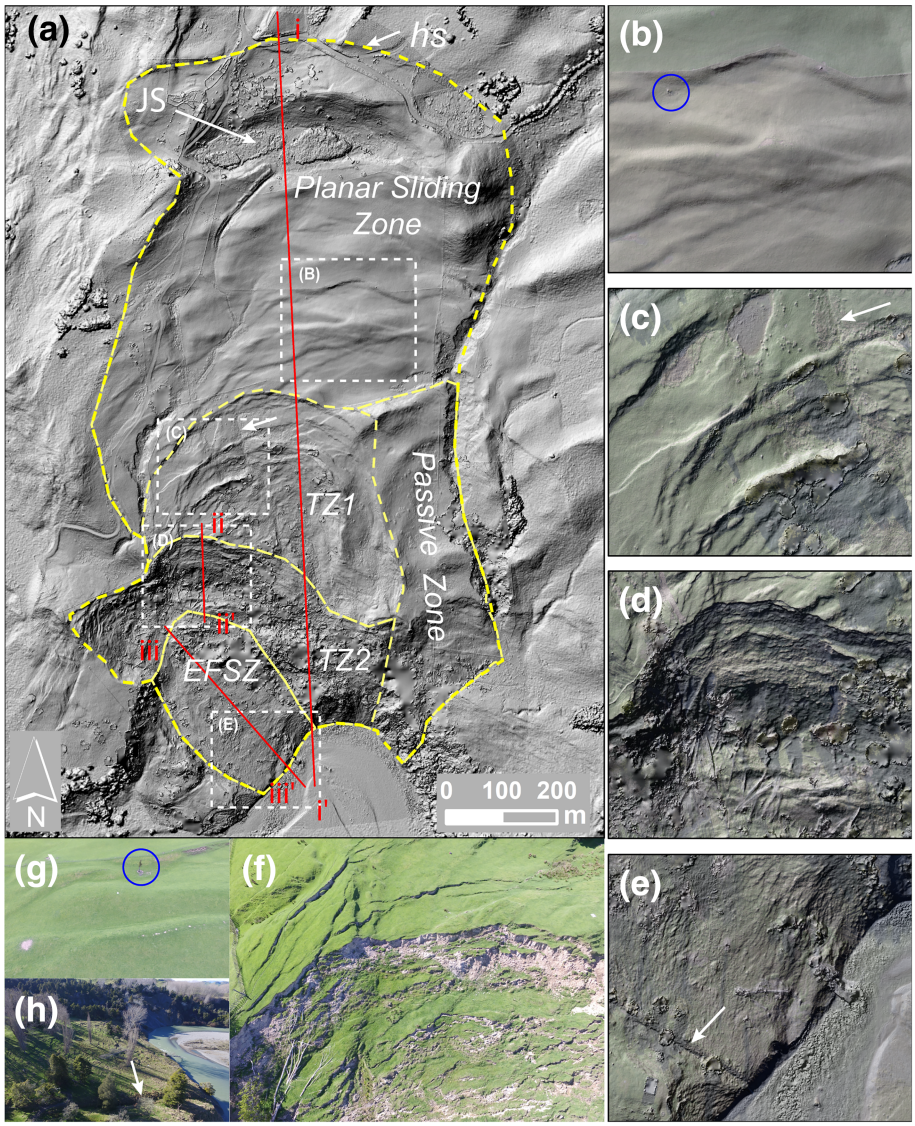

FIGURE 4 (a) Morphology of the Rangitikei Landslide with delineation of the landslide boundary and zones of characteristic movement style or mechanism (dashed yellow polygons; TZ = transitional zone; EFSZ = earthflow-sliding zone). Background image is a hillshade model from the May 2017 SfM DEM of this study or Horizons DEM beyond the landslide boundaries. JS = John's Swamp and *hs* = head scarp. The white dashed boxes correspond to panels B–E showing morphological features of interest, with the 2017 orthophoto mosaic beneath transparent hillshade model. Cross-section locations for Figure 5 are shown with red lines. (b) Example of a graben with relatively smooth scarps (indicating low movement rate/magnitude). (c) Example of a strongly developed graben, with high downhill-facing arcuate scarps. The white arrow points to a north–south-oriented structure dissecting this zone, also indicated at the same position by the white arrow in panel a. (d) Lower transitional zone 1 and transitional zone 2 with intense ground damage from vertical land movement and slumping. (e) The earthflow-slide zone at the landslide toe with a sharp, linear, landslide boundary indicated by the white arrow. Panels f and g provide a different (i.e. oblique) perspective of some of the same features. (f) An oblique aerial photo view of approximately the same area as panel d, showing both of the transitional zones in the western part of the landslide. (g) Oblique aerial photo of the same graben shown in panel b, with the same tree marked by the blue circle. (h) An oblique view looking east across the toe of the landslide with the landslide boundary marked by a white arrow [Color figure can be viewed at wileyonlinelibrary.com]

the landslide suggest a transition from dominantly brittle failure (sliding in PSZ) to more ductile deformation (flow) towards the toe of the landslide (Figure 4). Transitional zone 1 (TZ1) is slightly steeper than the PSZ and is characterized by nested arcuate SSE-facing scarps, several of which form well-developed but asymmetrical graben structures (Figure 4c). An approximately north–south-oriented linear structure dissects the zone (Figures 4a and c) and the scarps are more developed (higher and fresher) west of this structure. The eastern side of the landslide adjacent to TZ1 is characterized by more subtle scarps and morphology, suggesting less deformation, and is referred to as the 'passive zone' (Figure 4).

An increase in slope gradient at a prominent convex break in slope marks the boundary between TZ1 and TZ2 in the western part of the landslide (Figures 4 and 5). The break in slope can be traced east of the landslide, suggesting its origin as a former terrace riser. The zone is characterized by south-facing arcuate scarps that are less continuous and more closely spaced than in TZ1 and are mostly downhill facing (Figure 4d). In the western part of TZ2 the scarps are more active (fresh and broken) and are overall more numerous than in the eastern part of the zone, which extends downslope to the river where the toe of the landslide forms a steep bedrock slope. The boundary of the landslide on the western side juts out westward,

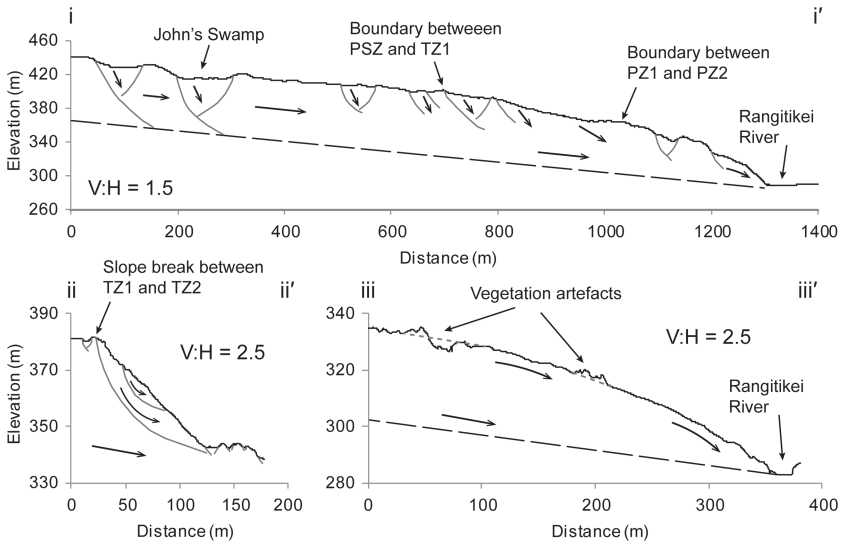

FIGURE 5 Topographic cross-sections along the (i–i′) whole landslide; (ii–ii′) transitional zone 2; and (iii–iii′) earthflow-slide zone, in locations given in Figure 4. The vertical scale is exaggerated in all sections; sections ii–ii′ and iii–iii′ use the same vertical exaggeration (V:H ratio of 2.5) with a vertical axis length of 60 m, whereas section i–i′ uses a ratio of 1.5 and a vertical axis length of 200 m. The dashed sub-horizontal line represents an approximation of the inferred sliding surface of the landslide (up to ~70 m below the ground surface, which is of a similar depth found for parts of the neighbouring Utiku Landslide; Massey, 2010), for which the dip angle corresponds approximately to the apparent general dip of bedding in the region. Arrows indicate the dominant movement directions indicated by morphological structures

TABLE 1 DEM error assessment for each photogrammetry survey using independent check points from RTK GPS survey

Survey	October 2016	May 2017	October 2017
Number of independent check points	14	17	22
Max vertical difference	0.302 m	0.481 m	0.945 m
RMSE of vertical difference	0.165 m	0.174 m	0.301 m
Arithmetic mean of vertical difference	0.018 m	0.032 m	0.140 m
Min vertical difference	0.029 m	0.001 m	0.011 m

cutting into the hillslope and extending the width of the landslide in this location, with eastward-facing scarps.

The western part of TZ2 grades into the earthflow-slide zone (EFSZ) which connects to the Rangitikei River (Figure 4). The EFSZ is more gently sloping (7°) than TZ2 (27°), but gradually steepens downslope in a convex form towards the river (Figure 5; xs iii–iii′). The lateral boundary of the EFSZ is well defined on the west with a prominent lateral shear (Figure 4e), but is less defined on the east where deformation is probably distributed more widely as it connects into the eastern part of TZ2. The ground in the EFSZ is highly disturbed and the materials are likely to have undergone sufficient remoulding (loss of cohesion) to allow them to flow, as indicated by the convex shape in the cross-section (Figure 3d). However, the well-defined lateral shear (i.e. indicative of brittle deformation), evidence of brittle fracture within the landslide body (i.e. multiple small-scale grabens), a well-defined failure surface exposed in the riverbank at the landslide toe, and other observations (described below) suggest that this zone also experiences basal sliding.

4.2 | DEM analysis

4.2.1 | DEM data quality

The errors in the DEMs evaluated from independent check points range from a minimum of 0.001 m to a maximum of 0.945 m, with RMSEs of 0.165, 0.174, and 0.301 m for October 2016, May 2017, and October 2017, respectively (Table 1). The RMSE values are inflated by high error at the landslide toe as a result of (up to ~0.5 m of) movement in the periods between the GPS surveying taking place (in the morning) and the photo collection (in the afternoon). If independent check points collected near the toe of the landslide are removed, then the maximum and RMSE values reduce to about one-third. The RMSE values are therefore considered conservative estimates of mean error for most parts of the model beyond the landslide toe. However, the RMSE errors are half to one-third of the maximum measured error, and therefore there are places in the model with considerably higher error.

4.2.2 | DoD analysis; geomorphic change and volumetric change assessment

Over the course of 1 year there was negligible detectable change over the upper (PSZ) zone of the landslide, and so our DoD analyses are focused on changes in the lower part of the landslide only (i.e. the transitional zones and EFSZ of Figure 4). Almost 50% of the lower part of the landslide body had detectable change, mostly in the form of surface lowering (Figure 6; Table 2), but with differences between the first DoD (October to May; i.e. summer) and the second (May to October; i.e. winter). Overall, more lowering is apparent in the winter DoD, whereas in the summer DoD these areas experienced mostly elevation gain. In both DoDs there is lowering at the toe of the landslide, but the magnitude and extent of lowering are larger in the winter (Figure 6).

An annual (October 2016–October 2017) thresholded volumetric change for the lower zones of the landslide (except for masked areas, e.g. trees) was calculated as −43 600 (±25 900) m^3. This represents a net elevation/volumetric loss (with the error value calculated by GCD

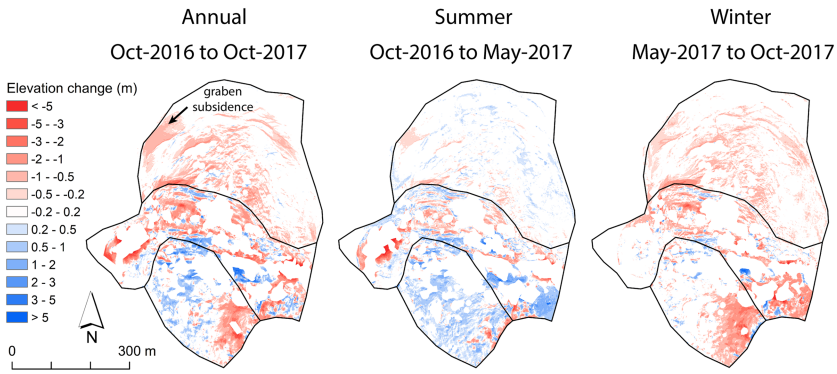

FIGURE 6 DEMs of difference over a full year (October 2016–October 2017) and within a year (i.e. summer, October 2016–May 2017 and winter, May 2017–October 2017) for the transitional and earthflow-slide zones of Rangitikei Landslide. Red pixels represent negative elevation changes (i.e. lowering) and blue pixels represent positive elevation changes (i.e. raising). The white areas represent locations where the elevation differences are less than the minimum level of detection from the propagated error (i.e. propagated RMSE from each survey) or where trees have been masked out (mainly in the lower zones of the landslide; Figure 3b) [Color figure can be viewed at wileyonlinelibrary.com]

TABLE 2 DEM of difference volumetric calculations for the transitional and earthflow-slide zones of the Rangitikei Landslide. The area of interest is the total area of cells differenced between the two DEMs, with the amount of detectable change within that area given in parentheses. All volumetric values presented are the thresholded values (using propagated error masks), such that cells that have change below this minimum level of detection threshold are ignored. For cells that have change above this threshold, only change exceeding the threshold is used. All values are rounded to the nearest 100 m^2 or 100 m^3. The negative sign for the net volume difference indicates volume reduction (i.e. lowering/erosion)

DoD epoch	Area of interest (m^2) and proportion of detectable change (%)	Volume of lowering (m^3)	Volume of raising (m^3)	Net volume difference (m^3)
Oct 2016 to Oct 2017 (annual)	206 600 (46%)	66 500 ± 24 700	22 900 ± 7900	−43 600 ± 25 900
Oct 2016 to May 2017 (summer)	199 700 (39%)	22 000 ± 6400	32 500 ± 12 200	+10 400 ± 13 800
May 2017 to Oct 2017 (winter)	192 100 (42%)	57 000 ± 25 000	7700 ± 2900	−49 300 ± 25 200

as the area of cells with detectable change multiplied by the RMSE errors propagated from Table 1). If the annual DoD volumetric change of 43 600 m^3 is converted into yield in tonnes, using a unit weight of 2 t/m^3 for remoulded landslide debris (from a neighbouring landslide; Massey, 2010), the yield is ~87 200 (±51 800) tonnes. The large percentage of error reflects a large number of cells with a small magnitude of change, expected for a mostly translational style of movement. Given that tree cover resulted in masking of about half of the lower zones, and the mLoD approach used ignores small changes, the annual yield is probably best considered to represent a minimum from this method. The thresholded volumetric change over the October 2016–May 2017 summer was +10 400 (±13 800). Although the error for the summer DoD exceeds the magnitude of change, there is a widespread pattern of elevation gain across much of the lower landslide in the summer (Figure 6), of a magnitude that is verified by checking against independent GPS data (i.e. GCPs and survey pegs) in this area of the landslide. Regardless of high uncertainty in the summer DoD, the winter (May 2017–October 2017) DoD gave a volumetric change of −49 300 (±25 200) m^3, suggesting that much more of the annual change (i.e. net lowering) occurred during the winter.

4.3 | Survey peg movement data; spatial distribution of movement

The GPS tracking of survey pegs at repeat survey intervals has confirmed that the whole landslide is actively moving downslope towards the Rangitikei River (Figure 7; Supplementary Table S2). Annual net displacements range from a mean of 0.2 m (max = 0.4 m) in the PSZ to 9.4 m (max = 18.1 m) in the EFSZ (Supplementary Table S2). The maximum cumulative net displacement for any one peg was 49 m (for Peg 22, over ~2.7 years between July 2015 and March 2018 before the peg was lost into the river; Figure S1). Peg 21 recorded the second largest cumulative net displacement, moving 44 m over an ~4.5-year period (Figure S1). The horizontal displacement directions (trends) are generally south but closer to the river they are rotated anticlockwise. They have a SSW azimuth (195°) in the PSZ, deviating westwards of the slope direction. The displacement direction is more due south in the transitional zones (183–188°). The direction is SE (156°) in the EFSZ (Figure 7), more parallel to the direction of slope. The vertical displacement is negative (i.e. vertically downwards), ranging from −13 to −16° in the PSZ and TZ1, to −22° in TZ2 and −5° in the EFSZ. Outside of the inferred landslide boundary, the annual net displacement rates are generally less than, but of a consistent order of magnitude (mean = 0.05 m/yr, max = 0.1 m/yr) to, pegs within the slowest landslide zone (the PSZ). The mean azimuth (229°) is more westward and the inclination shallower (9°) than the PSZ.

4.4 | Temporal patterns of movement and relationships to hydrological variables

The landslide movement varies through time, with a pronounced seasonality in displacement rates, such that displacement rates are faster in the late winter and spring months than in the summer and autumn

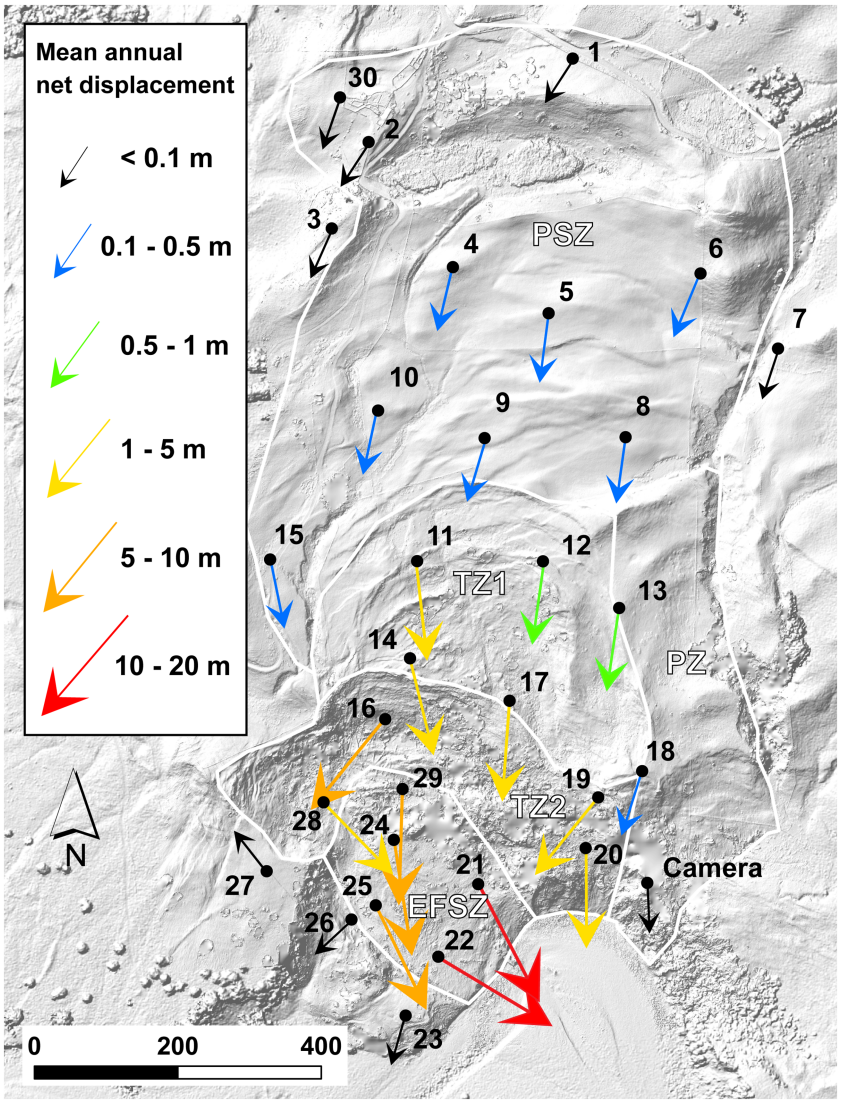

FIGURE 7 Mean annual net displacement rate (metres per year) of the survey pegs (black dots) from repeat RTK GPS surveys, from the first to the last observation of each peg. The displacement rate shown is not to scale (i.e. the arrow size is not to scale), but they show the overall pattern of displacement rate variation at locations on and around the landslide [Color figure can be viewed at wileyonlinelibrary.com]

(Figure 8). Displacement is on average 2.3 times faster at the start of summer than at the end of summer across all zones and years (2015–2016 = 1.8; 2016–2017 = 2.8; 2017–2018 = 2.2), with little difference between zones, and with five pegs having rates four to six times faster (Figure 8). Generally, for most years and zones the peak rates had established by October and declined thereafter through the summer, but in 2015 the peak rates for the PSZ and the EFSZ were later (~December). For the summer of 2016–2017, the same delay is seen for the PSZ but not for the EFSZ. The timing of the (true) peak rates of displacement after 2018 is less precise due to the reduction in the frequency of data collection. The seasonal changes in movement rate tend to mimic a seasonal pattern seen in both rainfall and river flow data, with a wetter winter and spring compared to summer (Figures 8 and S2). The relationship, however, is more pronounced for flow than for rainfall. For example, while flow rates and movement rates reduced during the summer of 2017/2018, there was not a notable drop in rainfall. This suggests that despite elevated local rainfall, the rainfall in the headwaters followed the usual seasonal reduction, causing a drop in flow and landslide movement (Figure 8). Inter-annual variability in movement also matches variability in both rainfall and flow, for example the EFSZ and TZ2 had higher movement rates in 2015 compared with 2016, consistent with a large cumulative deviation from mean daily rainfall and flow in 2015 (Figures 8 and S2). There was a trend of increasing movement after 2016 (e.g. winter peaks in movement rate nearly double between 2015 and 2017 in TZ1 for survey marks 11 and 14; Figure 8). This trend matches a trend of increasing rainfall and flow between 2016 and 2019, which declines, along with movement rates, after 2019 (Figures 8 and S2). The winter peak in movement rate for 2018 appears lower than previous years for most zones, but this is likely due to the longer interval between surveys, corroborated by the cumulative movement data. Furthermore, the seasonal minima (i.e. the movement rates at the slowest part of each year) seem to be increasing in all zones until 2019.

Displacement tracking in the EFSZ using time-lapse photography (see Supplementary Data Video) over a 1-year period further highlights the seasonality of displacement and the relationship between movement and hydrological variables (Figure 9). Cumulative flow and displacement both share a sharp increase in late winter to early spring (August–September), with cumulative rainfall following less closely, with a more gradual increase (Figure 9a). During the late autumn to early winter (May to July), displacement appears to be relatively insensitive to increases in either cumulative rainfall or flow (Figure 9a). During the summer to autumn months individual rainfall and flow events tend to cause small spikes in movement, but the largest daily rainfall values in the record (in November and December

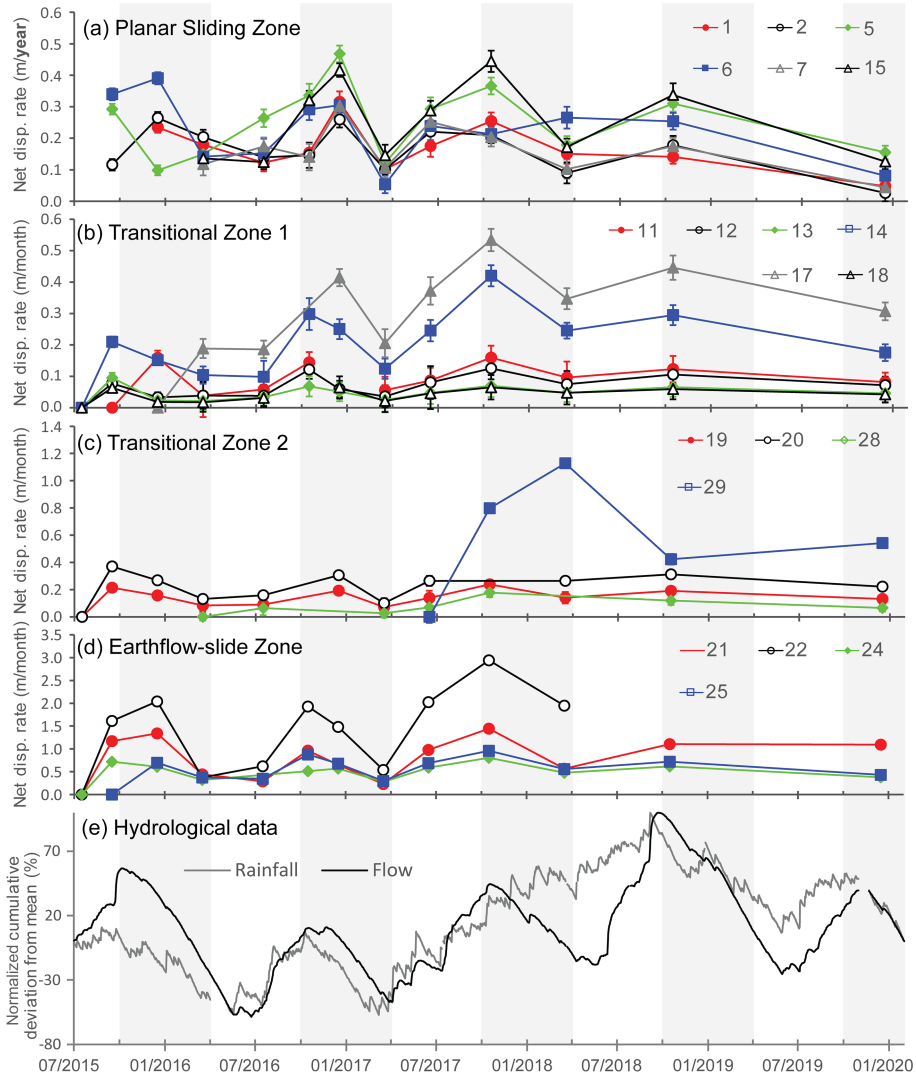

FIGURE 8 RTK GPS survey peg monitoring results plotted alongside hydrological data. Net displacement refers to the net of horizontal and vertical components of displacement and is plotted for selected pegs in the: (a) planar sliding zone; (b) transitional zone 1; (c) transitional zone 2; and (d) earthflow-slide zone. The vertical scale is different in each zone, and for the PSZ the units are in metres per year, whereas all other zones are metres per month. Error bars (vertical GPS precision + 1 cm pole placement allowance) are drawn on all plots but not all are visible due to the small error relative to the magnitude of displacement. See Supplementary Figure S1 for equivalent cumulative net displacement data. Panel (e) shows normalized cumulative deviation from mean rainfall (grey) measured at Taihape rec (agent 3671) rain gauge (~9 km northwest of the landslide) and river flow (black) measured at Mangaweka gauging station (~7 km southwest of landslide). See Supplementary Figure S2 for daily rainfall and flow data and further explanation of panel (e). The vertical grey bars indicate the summer half of the year (between October and March inclusive) [Color figure can be viewed at wileyonlinelibrary.com]

2015, i.e. in the summer) caused relatively small spikes in displacement (Figures 9a and b). In comparison, a large (>150 m^3/s) flood on 9 July, not associated with a large amount of local rainfall (instead driven by headwater rainfall), caused a large spike in displacement. Further spikes in movement during the winter period are associated with floods, some of which coincide with high local rainfall. In the spring (September and October), several further floods in excess of 100 m^3/s produced only slight increases in movement rate. Examining relationships between displacement data and that of rainfall and flow suggests that, during the 1-year monitoring period, displacement correlated more strongly with flow than rainfall (Figures 9c and d).

The two piezometers (P1 and P2) provide a record of groundwater levels in the EFSZ of approximately 6 and 12 months duration, respectively. The record from P2 is shorter due to damage from landslide movement (Supplementary Figure S3). Both piezometers experienced a reduction in water level through the summer of 2017/2018, with a minimum in early autumn 2018. The water level of P1 then rises to a maximum in the winter of 2018 and thereafter declines towards the end of the record in November (Supplementary Figure S2a). The seasonal pattern in water level shows a weak relationship with the cumulative deviation in mean rainfall (recorded at Taihape), but short-term peaks in water level correspond to major rainfall events (Supplementary Figure S2a and b). Movement rates of the EFSZ in proximity to P1 broadly follow the same seasonal pattern of higher movement in winter and spring to that of our other monitoring periods and datasets (cf. Figures 8 and 9), and this is consistent with the seasonal trend in water level recorded by P1 and P2. However, at an event-based level (i.e. weekly records from November 2017 to November 2018) there is no correspondence of movement pattern to the mean water level ($R^2 = 0.004$) and only a weak correlation ($R^2 = 0.192$) to mean rainfall (Figure 10a) of the previous 7-day interval. In contrast, there is a moderate correlation ($R^2 = 0.552$) between movement and mean Rangitikei River flow (recorded at Mangaweka) of the following 7 days. When divided between summer–autumn and winter–spring, two distinctive relationships with flow emerge, with a stronger and more positive correlation for the wetter months of the year, albeit largely as a result of two weeks in winter/spring with average flows in excess of 300 cumecs (Figure 10b). To explore the effect of a longer moving average, we also examined relationships between movement and the preceding 14, 21, and 28-day mean flow, rainfall, and water level, but in all cases the strongest correlations exist for flow (Supplementary Table S3).

4.5 | Sediment delivery to Rangitikei River

This sediment delivery estimate from DoD volumetric analysis can be independently evaluated using movement monitoring data.

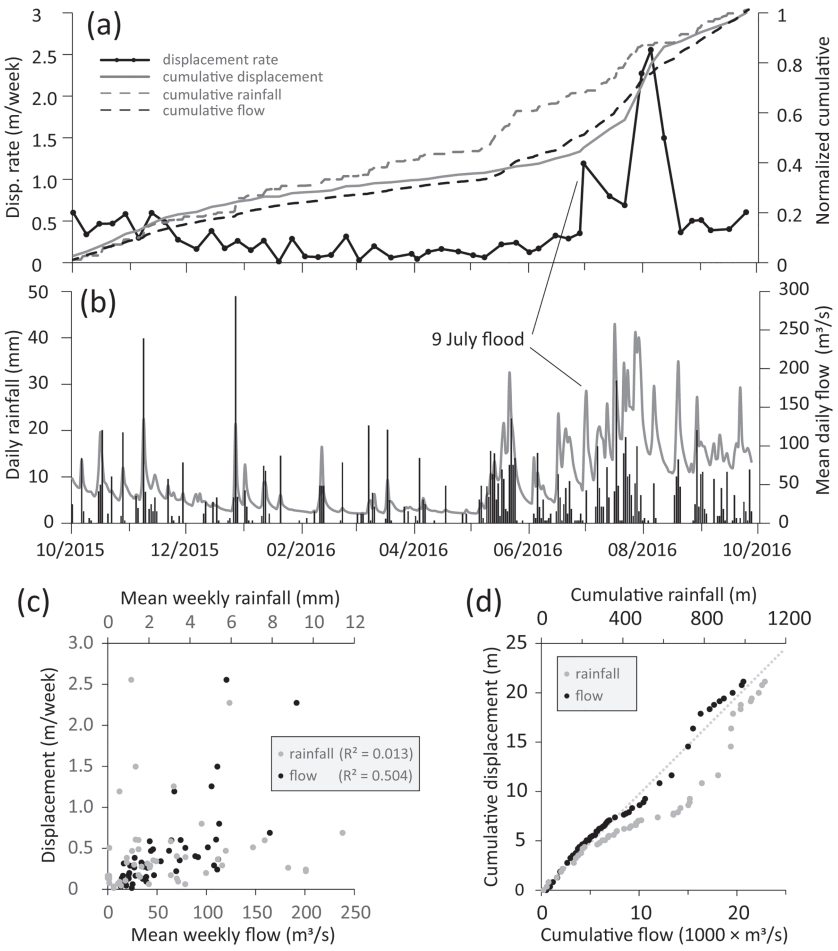

FIGURE 9 (a) Displacement rate (solid black line) of the lower central part of the earthflow-slide zone over 1 year from October 2015 to November 2016, from time-lapse photography pixel tracking using an ~7-day sampling interval. Normalized cumulative displacement (solid grey) is plotted alongside normalized cumulative daily rainfall (dashed grey) at Taihape and normalized cumulative daily flow (dashed black) of the Rangitikei River at Mangaweka (see Figure 1b for gauge locations). (b) Daily rainfall (black bars) and daily flow of the Rangitikei River (grey line). (c) Relationship between (pixel-tracking) displacement rate at a weekly interval and mean rainfall (of the previous 7 days) and mean river flow (of the previous 7 days). (d) Relationship between (pixel-tracking) cumulative weekly displacement and cumulative weekly rainfall and cumulative weekly flow. Grey dotted line indicates a 1:1 relationship for reference

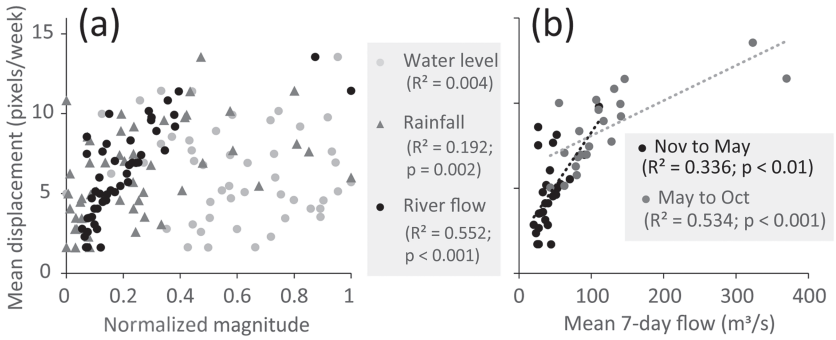

FIGURE 10 (a) Relationships between mean pixel displacement (at approximately weekly intervals) in proximity to piezometer 1 and that of mean water level, rainfall, and river flow of the preceding 7 days, from November 2017 to November 2018. The datasets are normalized to a maximum value of 1 to permit plotting on the same axis. (b) The relationship between mean pixel displacement and river flow presented separately for summer–autumn (November to May; black dots) and winter–spring (May to October; grey dots). See Supplementary Figure S2 for the equivalent time-series datasets

Assumed to be representative of movement near the toe, Pegs 21 and 22 in the EFSZ give an annual displacement of ~14 m. Holdsworth (2018) previously measured the width of the earthflow slide to be 156 m, and visual inspection of the river bank in this location suggests the thickness at the toe to be ~6 m. A movement rate of 14 m/yr results in an annual sediment delivery of 13 100 m^3 (or 26 200 tonnes using a unit weight of 2 t/m^3). In addition, there is a further ~100 m of landslide toe associated with the western part of TZ2. The DoD analysis and the movement pegs in that area suggest several metres of displacement annually (Figures 6 and 7; Peg 20 moves 3 m/yr). The toe in this location forms a steep slope/cliff about 25 m high. Assuming movement of Peg 20 is representative of the annual erosion at this location, this area is delivering a further 7500 m^3 (15 000 tonnes) of sediment per year. This takes the total estimated from the GPS movement measurements to (20 600 m^3) 41,000 t/yr, which is within (but at the lower end of) the range estimated from the annual DoD for the lower zones (17 700–69 500 m^3; or 35 400–139 000 t).

5 | DISCUSSION

5.1 | Landslide failure mechanism

Rangitikei Landslide has been preconditioned by weak, dipping bedrock layers, made unstable by the removal of toe support from fluvial erosion. This is consistent with site investigations of other nearby landslides (namely the Taihape and Utiku landslides; Massey et al., 2013, 2016) and landslide susceptibility modelling in the region, whereby the intersection of inclined strata and fluvially incised valleys is a first-order control on their development (Williams et al., 2021). The instability of the PSZ, with a gentle surface gradient (of 3–4°) and the dominance of horizontal extension and brittle response (e.g. grabens and sub-horizontal displacement vectors) are consistent with translational sliding along a gently inclined, weak failure surface (Massey, 2010). The GPS displacement vectors on and around the Rangitikei Landslide are also suggestive of translational sliding along bedding. Vectors in the PSZ, and of pegs outside the inferred landslide boundary, have a south to southwest direction (mean of 195 and 229°, respectively), parallel to the expected dip direction of the strata and deviating from the (south-facing) slope aspect. The vertical displacement vectors (13–16°) of the TZ1 and PSZ provide a reasonable approximation of the likely maximum (steepest) angle.

The landslide morphology, mechanism, and movement behaviour change downslope. There is a downslope increase in the morphological expression (e.g. intensity of ground damage, freshness and density of scarps), along with faster movement rates. There is an increase in vertical displacement (mean of −16° in the PSZ, increasing to −22° in the TZ2), and a rotation of the horizontal GPS movement vectors to a direction more similar to the slope aspect and more perpendicular to the river. The same anticlockwise rotation of pegs closer to the river is not seen for the pegs outside the landslide boundary. It can be inferred that these changes in landslide morphology and behaviour are in response to topographic forcing (i.e. river incision). This is reflected by a transition to more flow-like morphology at the toe from strain softening. The convex long profile in the EFSZ suggests a more ductile (i.e. remoulded, strain-softened) material that is responding to shear stresses imposed by the surface gradient that increases towards the river. A similar transition from planar sliding in the upper landslide to earthflow behaviour near the toe was observed at Utiku Landslide (Massey et al., 2018a). Furthermore, at Utiku Landslide the dominant landslide motion is not down-dip but instead along-strike, towards the Hautapu River, facilitated by ductile deformation (Massey, 2010). Both the Utiku and Rangitikei landslides therefore point to the strong influence that topographic forcing by fluvial incision has in destabilizing landslides and influencing behaviour.

The dominant role of the river at the Rangitikei Landslide in the present day likely reflects the current alignment of the Rangitikei River. Bend development has migrated the channel to the true right of the valley floor so that the toe of Rangitikei Landslide now abuts a sharp outside bend of the river, where the erosional capacity of the river is at its highest. Based on historical aerial photography from 1952 AD, the current river alignment has deviated little in historical times because the valley floor is relatively narrow in this confined setting. Paleochannel alignments along the river corridor suggest that over longer timeframes the channel position has migrated, such that the focus of bank erosion and movement rates of the landslide have likely changed. Indeed, some of the other landslides recognized within the Poroa Landslide Complex (e.g. ~1.5 km east of Rangitikei Landslide; Figure 2b) appear to be inactive with a degraded morphology and are no longer directly connected to the river. This mix of active and inactive landslides highlights the role played by lateral changes in the Rangitikei River alignment in switching on and off deep-seated landslide sediment delivery in the catchment.

5.2 | Temporal patterns of movement and the response to fluvial erosion

Measured temporal patterns of movement also point to the importance of fluvial erosion processes. There is a strong seasonal pattern to movement throughout the landslide, with elevated displacement rates during the winter and spring. While rainfall (therefore porewater pressure) likely modulates these patterns, as is found for many active landslides (e.g. Bennett et al., 2016b; Schulz et al., 2017), fluvial erosion appears to strongly influence movement rate, especially at the landslide toe. At sub-seasonal and weekly (i.e. flood event) timescales, there is a stronger relationship between landslide movement and flow data (measured at Mangaweka) than for rainfall (measured at Taihape) or groundwater level (measured in the EFSZ). The relationship between movement and river flow is considered to arise primarily due to bank erosion. Trimming of the bank during floods is observed in time-lapse photography (Supplementary Figure S4), and initiation of earthflow motion and slumping occur during the flood, suggesting bank erosion (rather than rapid drawdown) is the primary mechanism of destabilization.

Seasonal patterns in landslide movement have been observed at other similar landslides in the region (Massey et al., 2013), with the role of seasonal changes in porewater pressures in modifying stability and sliding having been demonstrated in laboratory experiments (Carey et al., 2019). Such studies have not explicitly evaluated the contribution of fluvial erosion in influencing movement patterns, however, the role of fluvial incision in priming failure is recognized (Massey et al., 2018a). During the 2004 Manawatū flood, erosion of the toe of Taihape Landslide by O'Taihape Stream destabilized the hillslope, resulting in a period of faster movement for several years thereafter (Massey et al., 2016). While it remains uncertain as to why the Rangitikei Landslide entered a phase of faster movement around 2015, we advance these studies by showing the importance of fluvial incision for the movement dynamics at annual, seasonal, and weekly (flood-event) timescales. Due to the disconnect between river flow (driven mostly by headwater rainfall) and 'local' rainfall (albeit measured a few kilometres to the north of the landslide but at a similar distance to the headwater ranges), we can identify events in which the landslide responds to flooding (i.e. bank erosion) without any notable 'local' rainfall. Furthermore, while more robust analyses would be required to assess the relative importance of rainfall or groundwater in controlling the movement patterns of the landslide as a whole (e.g. Van Asch et al., 2007), we show these factors to be of lesser importance than fluvial erosion in controlling weekly to seasonal movement dynamics at the highly sensitized toe of the Rangitikei Landslide. Our data suggest that the highly coupled mobile landslide toe is extremely sensitive to erosion by the river, such that the pace of movement varies closely with river flow (i.e. bank erosion),

perhaps to the point where fluctuations in porewater pressure have relatively little influence on the movement pattern in that location.

We also show how the sensitivity to both rainfall and river flow changes throughout the year, with the highest sensitivity occurring in winter and spring. Following major movement episodes in spring, we see a reduction in sensitivity at the toe of the landslide, perhaps suggesting that the EFSZ has to be 'recharged' by material from the transitional zone before it becomes sensitive again. A recharge phenomenon may explain why we observe surface elevation gains across the lower half of the landslide during the summer months (October to May) in the DEM differencing. This is unlikely to be related to surface inflation from seasonal shrink–swell effects observed elsewhere (Massey et al., 2013), as the signal is opposite to what is expected (i.e. surface lowering from shrinkage would be expected during summer). Another contribution to this 'recharge' effect could be from movement of the wider Poroa Landslide Complex. Our movement pegs, outside the morphologically defined landslide boundary, show small but persistent displacement in the SSW direction. Resolving whether such movement reflects Poroa Landslide Complex movement or poor definition of the Rangitikei Landslide boundary will require a more extensive monitoring network.

Our findings build on a body of work that points to the importance of fluvial erosion in driving landslides. At the orogen and catchment scale, the intensity of fluvial incision influences the distribution of landslides and landslide activity (e.g. following post-glacial incision) (Bilderback et al., 2014; Larsen & Montgomery, 2012; Roering et al., 2015). Within the Whanganui–Rangitikei region, river incision (i.e. incised topography) is a strong predictor of the spatial distribution of large landslides (Williams et al., 2021). Our research suggests that this not only manifests through kinematic feasibility (i.e. susceptibility), as suggested by the deviation in movement vectors towards the actively eroding landslide toe, but fluvial erosion processes also influence the movement rates of active landslides at multiple timescales. In other places, waves of movement associated with fluvial incision have been identified in the lower zones of earthflows (Nereson & Finnegan, 2018), but here we show fluvial incision to be a persistent control on movement. From the data available it is difficult to relate the changes in movement patterns of the upper parts of the landslide to toe erosion to assess how far and over what timescale the toe erosion signal propagates. However, several observations suggest that the effects of toe erosion are felt throughout the landslide body; extensional strain in the upper landslide, a similar seasonal pattern in movement in the upper landslide but of lower magnitude to the lower landslide, and a downslope increase in movement rates. Provided that the present river alignment remains, it is likely that the landslide will continue to move in response to bank erosion, and this will drive retrogression (and upslope enlargement) of the transitional zones.

5.3 | Sediment delivery—nature and significance

Our results suggest that Rangitikei Landslide is delivering a considerable volume of sediment into Rangitikei River. Two independent calculations of delivery (survey peg movement data and DEM differencing) with an overlapping error range provide confidence in this finding. We consider 40 000 tonnes to be a realistic and probably conservative estimate of annual sediment delivery from the landslide. This volume represents 7% of the measured annual suspended sediment load of the Rangitikei catchment (Dymond et al., 2016). Given that the landslide occupies only 0.03% of the catchment area, this is a highly disproportionate point source of sediment delivery to the river. Due to the dominantly fine-grained bedrock and remoulded (i.e. weakened and disaggregated) landslide toe material, most of the sediment being delivered to the river is readily entrained and breaks down rapidly. These sediments are therefore contributing directly to the suspended sediment load, and have an immediate impact on water quality and ecological health (Ballantine et al., 2015; Davies-Colley, 2013). Landslides in the Neogene cover rocks, such as the Rangitikei Landslide, can deliver coarser clastic material (e.g. from carbonate or concretion-rich rocks translocation of river terrace gravels), but these tend to be minor constituents. As a consequence of this contribution to suspended load, the impact of these landslides on the fluvial system differs from that of many landslide terrains previously studied. In other landscapes, bedrock landslides and some earthflows deliver a high proportion of coarse (often bouldery), hard, clastic material. Delivery of such clastic material contributes dominantly to bedload, and can promote river incision (i.e. by providing erosion tools), and has a more pronounced impact on river morphology through occlusions, blockages, or changes in planform (Bennett et al., 2016a; Egholm et al., 2013; Finnegan et al., 2019; Korup, 2005; Korup et al., 2004; Shobe et al., 2021), but may have lesser impact on water quality.

There is a seasonal variability to the disproportionately high sediment delivery from Rangitikei Landslide. Landslide movement rates, and therefore delivery, vary by two to three times between the fastest (winter–spring) and slowest (summer–autumn) period. This is reflected by the DEM analysis, with contrasting changes (particularly in the lower landslide zones) between October–May (net surface gain) and May–October (net surface lowering). This difference is interpreted as the landslide responding to more rapid toe cutting by Rangitikei River during higher winter flows and more rapid and ductile (flow-like) deformation of the wetter earthflow-slide mass. Likewise, the surface lowering of the western part of TZ2 in the winter may represent more aggressive erosion by the river, while the surface raising in this part of the zone in the summer may represent ongoing landslide movement (i.e. recharge) with less effective fluvial erosion/removal of the material. Therefore, the majority of the sediment yield to the river is likely taking place over several of the wetter months of the year; but nonetheless, the landslide continues to deliver sediment, albeit at a slower rate, throughout the year and especially in response to major floods. This persistent, but seasonally variable, delivery of sediment from a large, slow-moving landslide contrasts with many other sources of mass movement erosion. Rainfall or earthquake-triggered landslides—the focus of much previous landslide erosion research—are associated with irregular, high-magnitude events. In Aotearoa, landslide-triggering storm events can occur at any time of the year, and the recurrence interval of major events (triggering thousands of landslides) at a regional scale tends to be decadal to centennial. For example, the 2004 Manawatū storm which generated some 62 000 mostly shallow landslides has an estimated 150-year return period (Dymond et al., 2006; Fuller & Heerdegen, 2005). Such storm events generate a major pulse of sediment delivery and although their effects can last years, they differ from the chronic delivery of slow-moving landslides.

Slow-moving landslides, like the Rangitikei Landslide, are likely to be a long-term source of sediment delivery. A conservative estimate of 50 m as an average depth for the 80-ha Rangitikei Landslide (Figure 5) equates to a volume of 40 M m^3. If the current delivery rate (~20 000 m^3/yr) was maintained, this would equate to another 2000 years before the landslide is exhausted. More likely, the landslide will fluctuate between periods of faster and slower movement (e.g. Bovis & Jones, 1992), with shifts in the position of the Rangitikei River, climate, and episodic earthquake activity. That, coupled with potential growth (e.g. by retrogression above John's Swamp), means the lifespan may greatly exceed 2000 years.

This study is one of the first to document the delivery rates of a contemporary (active) slow-moving landslide in Aotearoa's Neogene cover rocks. Previous work had evaluated the longer-term sediment contribution of large landslides and earthflows in Waipaoa catchment, East Cape and identified these to be a major source of sediment in the post-glacial period (Bilderback et al., 2014; Booth et al., 2013; Cerovski-Darriau et al., 2014; Marden et al., 2018; Zhang et al., 1991), but such work has not been extended elsewhere in Aotearoa or examined contemporary delivery. Future research should seek to quantify the movement and sediment delivery rates of the many thousands of other large landslides mapped within similar soft-rock terrain (Rosser et al., 2017; Williams et al., 2021), for which the activity status is unknown for the majority. This would help to assess whether the Rangitikei Landslide is an anomaly or characteristic, and try to quantify how sediment delivery from such landslides varies over space and time and what their overall contribution is to catchment sediment yields. If the Rangitikei Landslide is characteristic, then this type of landslide erosion process needs to be explicitly accounted for in erosion and sediment delivery models (e.g. SedNetNZ; Dymond et al., 2016) and considered within landscape management and sediment reduction strategies to meet national policy targets. Our research suggests that any efforts to try to reduce the movement of such landslides is probably best targeted at reducing fluvial incision/toe erosion; or at least not exacerbating incision like has been suggested of river gravel extraction below the Utiku Landslide (McSaveney & Massey, 2017) or quarrying at the toe of the Abbotsford Landslide (Hancox, 2008).

6 | CONCLUSIONS

The Rangitikei Landslide is an 80-ha translational landslide that transitions into an earthflow-slide at the landslide toe. We demonstrate that fluvial erosion is a dominant process driving instability, the evolution of morphology, and movement of a large, soft-rock landslide in Aotearoa. Due to strong coupling to the river, movement rates of the landslide toe closely correlate with river flow fluctuations over flood event to seasonal timescales. Our findings suggest that for highly coupled landslides, fluvial erosion can have considerable influence on the movement patterns and sensitivity of the landslide to other environmental variables such as porewater pressures. Furthermore, we determine that this highly coupled landslide is a major and previously unaccounted for source of fine-grained sediment to the Rangitikei River, delivering 7% of the estimated annual sediment load of the catchment from 0.03% of contributing catchment area. While the sources of error in both methods of calculation (surface movement and DEM differencing) are large, the conclusion is unavoidable that the landslide is delivering a large and disproportionate amount of sediment into the Rangitikei River on an annual (but seasonably variable) basis. While only a single example, it may be representative of many other mapped landslides that are actively connected to stream systems in Aotearoa's soft-rock hill country, or of similar landscapes elsewhere. Such landslide delivery and slope–channel coupling could constitute a major process of hillslope erosion, sediment delivery, and change in these landscapes.

ACKNOWLEDGEMENTS

We are grateful for funding support from a Canon Environmental Grant for the time-lapse camera equipment, the Eric Ojala Sub-Trust Grant for purchase of groundwater monitoring equipment, and funding from the New Zealand Ministry of Business, Innovation and Employment research program 'Smarter Targeting of Erosion Control (STEC)' (Contract C09X1804). We thank Horizons Regional Council for kindly providing their digital surface model, rainfall and river flow data, and for financially supporting Charlotte Holdsworth's MSc project. Charlotte's project was also supported by the British Society for Geomorphology Research Grant. Thanks are given to Libby Owen of Horizons Regional Council for fieldwork support and, along with Grant Cooper, helping to establish the project. We thank fieldwork assistants Andrew Nevermann, Jan Blahut, and Alastair Clement, and are grateful for the access and valuable local knowledge provided by the landowner. Graham Hancox is thanked for sharing his oblique aerial photographs. We thank Dr Saskia de Vilder and an anonymous reviewer for constructive and supportive reviews that have helped to improve the manuscript. Open access publishing facilitated by Massey University, as part of the Wiley - Massey University agreement via the Council of Australian University Librarians. [Correction added on 20 May 2022, after first online publication: CAUL funding statement has been added.]

CONFLICT OF INTEREST

The authors have no conflict of interest to declare.

FUNDING STATEMENT

All funding sources are mentioned in the Acknowledgements section.

DATA AVAILABILITY STATEMENT

Data produced in this research will be made available upon request where it is not provided within the manuscript or supplementary data resources.

ORCID

Samuel Thomas McColl https://orcid.org/0000-0002-2805-1761
Charlotte Naomi Holdsworth https://orcid.org/0000-0002-4572-3638
Ian Christopher Fuller https://orcid.org/0000-0002-5123-1648
Forrest Williams https://orcid.org/0000-0001-8721-6020

REFERENCES

Arsenault, A.M. & Meigs, A.J. (2005) Contribution of deep-seated bedrock landslides to erosion of a glaciated basin in southern Alaska. *Earth Surface Processes and Landforms*, 30(9), 1111–1125. Available from: https://doi.org/10.1002/esp.1265

Ballantine, D., Hughes, A. & Davies-Colley, R. (2015) Mutual relationships of suspended sediment, turbidity and visual clarity in New Zealand rivers. *Proceedings of the International Association of Hydrological*

Sciences, 367, 265–271. Available from: https://doi.org/10.5194/piahs-367-265-2015

Basher, L., Betts, H., Lynn, I., Marden, M., McNeill, S., Page, M. & Rosser, B. (2018) A preliminary assessment of the impact of landslide, earthflow, and gully erosion on soil carbon stocks in New Zealand. *Geomorphology*, 307, 93–106. Available from: https://doi.org/10.1016/j.geomorph.2017.10.006

Beetham, R.D., McSaveney, M.J. & Read, S.A.L. (2002) Four extremely large landslides in New Zealand. In: Rybar, J., Stemberk, J. & Wagner, P. (Eds.) *Landslides: Proceedings of the First European Conference on Landslides*. Lisse/Rotterdam: Swets and Zeitlinger/A.A. Balkema, pp. 97–102.

Bennett, G.L., Miller, S.R., Roering, J.J. & Schmidt, D.A. (2016a) Landslides, threshold slopes, and the survival of relict terrain in the wake of the Mendocino Triple Junction. *Geology*, 44(5), 363–366. Available from: https://doi.org/10.1130/G37530.1

Bennett, G.L., Roering, J.J., Mackey, B.H., Handwerger, A.L., Schmidt, D. A. & Guillod, B.P. (2016b) Historic drought puts the brakes on earthflows in Northern California. *Geophysical Research Letters*, 43(11), 5725–5731. Available from: https://doi.org/10.1002/2016GL068378

Bilderback, E.L., Pettinga, J.R., Litchfield, N.J., Quigley, M., Marden, M., Roering, J.J. & Palmer, A.S. (2014) Hillslope response to climate-modulated river incision in the Waipaoa catchment, East Coast North Island, New Zealand. *Geological Society of America Bulletin*, 127, 131–148.

Booth, A.M., Roering, J.J. & Rempel, A.W. (2013) Topographic signatures and a general transport law for deep-seated landslides in a landscape evolution model. *Journal of Geophysical Research – Earth Surface*, 118(2), 603–624. Available from: https://doi.org/10.1002/jgrf.20051

Bovis, M.J. & Jones, P. (1992) Holocene history of earthflow mass movements in south-central British Columbia: The influence of hydroclimatic changes. *Canadian Journal of Earth Sciences*, 29(8), 1746–1755. Available from: https://doi.org/10.1139/e92-137

Carey, J.M., Massey, C.I., Lyndsell, B. & Petley, D.N. (2019) Displacement mechanisms of slow-moving landslides in response to changes in porewater pressure and dynamic stress. *Earth Surface Dynamics*, 7(3), 707–722. Available from: https://doi.org/10.5194/esurf-7-707-2019

Cerovski-Darriau, C., Roering, J.J., Marden, M., Palmer, A.S. & Bilderback, E.L. (2014) Quantifying temporal variations in landslide-driven sediment production by reconstructing paleolandscapes using tephrochronology and lidar: Waipaoa River, New Zealand. *Geochemistry, Geophysics, Geosystems*, 15(11), 4117–4136. Available from: https://doi.org/10.1002/2014GC005467

Crozier, M.J. (2005) Multiple-occurrence regional landslide events in New Zealand: Hazard management issues. *Landslides*, 2(4), 247–256. Available from: https://doi.org/10.1007/s10346-005-0019-7

Crozier, M.J. & Pillans, B.J. (1991) Geomorphic events and landform response in south-eastern Taranaki, New Zealand. *Catena*, 18(5), 471–487. Available from: https://doi.org/10.1016/0341-8162(91)90050-8

Dadson, S.J., Hovius, N., Chen, H., Dade, W.B., Lin, J.-C., Hsu, M.-L., Lin, C.-W., Horng, M.-J., Chen, T.-C., Milliman, J. & Stark, C.P. (2004) Earthquake-triggered increase in sediment delivery from an active mountain belt. *Geology*, 32(8), 733–736. Available from: https://doi.org/10.1130/G20639.1

Davies-Colley, R.J. (2013) River water quality in New Zealand: An introduction and overview. In: Dymond, J.R. (Ed.) *Ecosystem Services in New Zealand: Conditions and Trends*. Lincoln, NE: Manaaki Whenua Press, pp. 432–447.

Dymond, J.R., Ausseil, A.-G., Shepherd, J.D. & Buettner, L. (2006) Validation of a region-wide model of landslide susceptibility in the Manawatu–Wanganui region of New Zealand. *Geomorphology*, 74(1–4), 70–79. Available from: https://doi.org/10.1016/j.geomorph.2005.08.005

Dymond, J.R., Herzig, A., Basher, L., Betts, H.D., Marden, M., Phillips, C.J., Ausseil, A.-G.E., Palmer, D.J., Clark, M. & Roygard, J. (2016) Development of a New Zealand SedNet model for assessment of catchment-wide soil-conservation works. *Geomorphology*, 257, 85–93. Available from: https://doi.org/10.1016/j.geomorph.2015.12.022

Edbrooke, S.W., Heron, D.W., Forsyth, P.J. & Jongens, R. (compilers) (2015) *Geological map of New Zealand 1:1 000 000*, Institute of Geological & Nuclear Sciences Geological Map 2. Lower Hutt, N.Z: GNS Science.

Egholm, D.L., Knudsen, M.F. & Sandiford, M. (2013) Lifespan of mountain ranges scaled by feedbacks between landsliding and erosion by rivers. *Nature*, 498(7455), 475–478. Available from: https://doi.org/10.1038/nature12218

Emberson, R., Hovius, N., Galy, A. & Marc, O. (2016) Chemical weathering in active mountain belts controlled by stochastic bedrock landsliding. *Nature Geoscience*, 9(1), 42–45. Available from: https://doi.org/10.1038/ngeo2600

Finnegan, N.J., Broudy, K.N., Nereson, A.L., Roering, J.J., Handwerger, A. L. & Bennett, G. (2019) River channel width controls blocking by slow-moving landslides in California's Franciscan mélange. *Earth Surface Dynamics*, 7(3), 879–894. Available from: https://doi.org/10.5194/esurf-7-879-2019

Fuller, I.C. & Heerdegen, R.G. (2005) The February 2004 floods in the Manawatu, New Zealand: Hydrological significance and impact on channel morphology. *Journal of Hydrology New Zealand*, 44, 75–90.

Hancox, G.T. (2008) The 1979 Abbotsford Landslide, Dunedin, New Zealand: A retrospective look at its nature and causes. *Landslides*, 5(2), 177–188. Available from: https://doi.org/10.1007/s10346-007-0097-9

Hancox, G.T. & Wright, K. (2005) *Analysis of Landsliding Caused by the 15–17 February 2004 Rainstorm in the Wanganui–Manawatu Hill Country, Southern North Island, New Zealand*, Report 2005/11. Lower Hutt, N.Z: GNS Science.

Holdsworth, C.N. (2018) The influence of rainfall and river incision on the movement rate of a slow-moving, soft rock landslide in the Rangitikei, New Zealand. Unpublished MSc Thesis, Massey University, Palmerston North, New Zealand, 135p.

James, M.R., How, P. & Wynn, P.M. (2016) Pointcatcher software: Analysis of glacial time-lapse photography and integration with multitemporal digital elevation models. *Journal of Glaciology*, 62(231), 159–169. Available from: https://doi.org/10.1017/jog.2016.27

James, M.R. & Robson, S. (2014) Mitigating systematic error in topographic models derived from UAV and ground-based image networks. *Earth Surface Processes and Landforms*, 39(10), 1413–1420. Available from: https://doi.org/10.1002/esp.3609

Korup, O. (2005) Large landslides and their effect on sediment flux in South Westland, New Zealand. *Earth Surface Processes and Landforms*, 30(3), 305–323. Available from: https://doi.org/10.1002/esp.1143

Korup, O. (2006) Rock-slope failure and the river long profile. *Geology*, 34(1), 45–48. Available from: https://doi.org/10.1130/G21959.1

Korup, O. (2008) Rock type leaves topographic signature in landslide-dominated mountain ranges. *Geophysical Research Letters*, 35(11), L11402. Available from: https://doi.org/10.1029/2008GL034157

Korup, O., Clague, J.J., Hermanns, R.L., Hewitt, K., Strom, A.L. & Weidinger, J.T. (2007) Giant landslides, topography, and erosion. *Earth and Planetary Science Letters*, 261(3–4), 578–589. Available from: https://doi.org/10.1016/j.epsl.2007.07.025

Korup, O., McSaveney, M.J. & Davies, T.R.H. (2004) Sediment generation and delivery from large historic landslides in the Southern Alps, New Zealand. *Geomorphology*, 61(1–2), 189–207. Available from: https://doi.org/10.1016/j.geomorph.2004.01.001

Larsen, I.J. & Montgomery, D.R. (2012) Landslide erosion coupled to tectonics and river incision. *Nature Geoscience*, 5(7), 468–473. Available from: https://doi.org/10.1038/ngeo1479

Larsen, I.J., Montgomery, D.R. & Korup, O. (2010) Landslide erosion controlled by hillslope material. *Nature Geoscience*, 3(4), 247–251. Available from: https://doi.org/10.1038/ngeo776

Lee, J., Townsend, D., Bland, K. & Kamp, P. (compilers)(2011) *Geology of the Hawke's Bay area*. Institute of Geological & Nuclear Sciences 1: 250,000 geological map 8; 93 pp. + 1 folded map. Lower Hutt, N.Z: GNS Science.

Lin, G.-W., Chen, H., Hovius, N., Horng, M.-J., Dadson, S., Meunier, P. & Lines, M. (2008) Effects of earthquake and cyclone sequencing on landsliding and fluvial sediment transfer in a mountain catchment.

Earth Surface Processes and Landforms, 33(9), 1354–1373. Available from: https://doi.org/10.1002/esp.1716

Litchfield, N. & Berryman, K. (2006) Relations between postglacial fluvial incision rates and uplift rates in the North Island, New Zealand. *Journal of Geophysical Research – Earth Surface*, 111(F2), Available from: https://doi.org/10.1029/2005JF000374

Mackey, B.H. & Roering, J.J. (2011) Sediment yield, spatial characteristics, and the long-term evolution of active earthflows determined from airborne LiDAR and historical aerial photographs, Eel River, California. *GSA Bulletin*, 123(7–8), 1560–1576. Available from: https://doi.org/10.1130/B30306.1

Marden, M., Fuller, I.C., Herzig, A. & Betts, H.D. (2018) Badass gullies: Fluvio-mass-movement gully complexes in New Zealand's East Coast region, and potential for remediation. *Geomorphology*, 307, 12–23. Available from: https://doi.org/10.1016/j.geomorph.2017.11.012

Massey, C., Abbott, E., McSaveney, M., Petley, D. & Richards, L. (2018a) Earthquake-induced displacement is insignificant in the reactivated Utiku landslide, New Zealand. In: Aversa, S., Cascini, L., Picarelli, L. & Scavia, C. (Eds.) *Landslides and Engineered Slopes: Experience, Theory and Practice*. Boca Raton, FL: CRC Press, pp. 31–52.

Massey, C., Petley, D. & McSaveney, M. (2013) Patterns of movement in reactivated landslides. *Engineering Geology*, 159, 1–19. Available from: https://doi.org/10.1016/j.enggeo.2013.03.011

Massey, C., Petley, D., McSaveney, M. & Archibald, G. (2016) Basal sliding and plastic deformation of a slow, reactivated landslide in New Zealand. *Engineering Geology*, 208, 11–28. Available from: https://doi.org/10.1016/j.enggeo.2016.04.016

Massey, C., Townsend, D., Rathje, E., Allstadt, K.E., Lukovic, B., Kaneko, Y., Bradley, B., Wartman, J., Jibson, R.W., Petley, D.N., Horspool, N., Hamling, I., Carey, J., Cox, S., Davidson, J., Dellow, S., Godt, J.W., Holden, C., Jones, K., Kaiser, A., Little, M., Lyndsell, B., McColl, S., Morgenstern, R., Rengers, F.K., Rhoades, D., Rosser, B., Strong, D., Singeisen, C. & Villeneuve, M. (2018b) Landslides triggered by the 14 November 2016 Mw 7.8 Kaikōura Earthquake, New Zealand. *Bulletin of the Seismological Society of America*, 108(3B), 1630–1648. Available from: https://doi.org/10.1785/0120170305

Massey CI. 2010. *The dynamics of reactivated landslides: Utiku and Taihape, North Island, New Zealand*. PhD thesis, Durham University. Available at http://etheses.dur.ac.uk/587/

McColl, S.T. & McCabe, M. (2016) The causes and agricultural impacts of large translational landslides: Case-studies from North Island, New Zealand. In: Aversa, S., Cascini, L., Picarelli, L. & Scavia, C. (Eds.) *Landslides and Engineered Slopes: Experience, Theory and Practice*. Boca Raton, FL: CRC Press, pp. 1401–1408.

McSaveney, M.J. & Massey, C.I. (2017) Inadvertent engineered activation of Utiku landslide, New Zealand. In: *Workshop on World Landslide Forum*. Cham: Springer, pp. 563–568. Available from: https://doi.org/10.1007/978-3-319-53487-9_66

Milne JDG. 1973. *Map and Sections of River Terraces in the Rangitikei Basin, North Island, New Zealand*. New Zealand Soil Survey Report 4.

Mountjoy, J. & Pettinga, J.R. (2006) Controls on large deep-seated landslides in soft rock terrain: Rock mass defects and seismic triggering. In: *Earthquakes and Urban Development: New Zealand Geotechnical Society Symposium*. Nelson, N.Z: Institution of Professional Engineers New Zealand.

Nereson, A.L., Davila Olivera, S. & Finnegan, N.J. (2018) Field and remote-sensing evidence for hydro-mechanical isolation of a long-lived earthflow in central California. *Geophysical Research Letters*, 45(18), 9672–9680. Available from: https://doi.org/10.1029/2018GL079430

Nereson, A.L. & Finnegan, N.J. (2018) Drivers of earthflow motion revealed by an 80 yr record of displacement from Oak Ridge earthflow, Diablo Range, California, USA. *GSA Bulletin*, 131, 389–402.

Rees, C., Palmer, A. & Palmer, J. (2020) Litho-structural controls on Quaternary landslide distribution in the Rangitikei hill country, North Island, New Zealand. *New Zealand Journal of Geology and Geophysics*, 63(1), 90–109. Available from: https://doi.org/10.1080/00288306.2019.1629966

Roering, J.J., Mackey, B.H., Handwerger, A.L., Booth, A.M., Schmidt, D.A., Bennett, G.L. & Cerovski-Darriau, C. (2015) Beyond the angle of repose: A review and synthesis of landslide processes in response to rapid uplift, Eel River, Northern California. *Geomorphology*, 236, 109–131. Available from: https://doi.org/10.1016/j.geomorph.2015.02.013

Rosser, B., Dellow, S., Haubrock, S. & Glassey, P. (2017) New Zealand's National Landslide Database. *Landslides*, 14(6), 1949–1959. Available from: https://doi.org/10.1007/s10346-017-0843-6

Schulz, W.H., Coe, J.A., Ricci, P.P., Smoczyk, G.M., Shurtleff, B.L. & Panosky, J. (2017) Landslide kinematics and their potential controls from hourly to decadal timescales: Insights from integrating ground-based InSAR measurements with structural maps and long-term monitoring data. *Geomorphology*, 285, 121–136. Available from: https://doi.org/10.1016/j.geomorph.2017.02.011

Shobe, C.M., Turowski, J.M., Nativ, R., Glade, R.C., Bennett, G.L. & Dini, B. (2021) The role of infrequently mobile boulders in modulating landscape evolution and geomorphic hazards. *Earth-Science Reviews*, 220, 103717. Available from: https://doi.org/10.1016/j.earscirev.2021.103717

Simoni, A., Ponza, A., Picotti, V., Berti, M. & Dinelli, E. (2013) Earthflow sediment production and Holocene sediment record in a large Apennine catchment. *Geomorphology*, 188, 42–53. Available from: https://doi.org/10.1016/j.geomorph.2012.12.006

Thomson RC. 1982. *Relationship of geology to slope failures in soft rocks of the Taihape–Mangaweka area, Central North Island, New Zealand*. PhD thesis, University of Auckland.

Townsend, D., Kamp, P. & Vonk, A. (2008) *Geology of the Taranaki area*. Institute of Geological & Nuclear Sciences 1:250,000 geological map 7, 77 pp. + 1 folded map. Lower Hutt, N.Z: GNS Science.

Van Asch, T.W., Van Beek, L.P.H. & Bogaard, T.A. (2007) Problems in predicting the mobility of slow-moving landslides. *Engineering Geology*, 91(1), 46–55. Available from: https://doi.org/10.1016/j.enggeo.2006.12.012

Wheaton, J. (2015) *Geomorphic Change Detection Software*. Logan, UT: Utah State University.

Wheaton, J.M., Brasington, J., Darby, S.E. & Sear, D.A. (2010) Accounting for uncertainty in DEMs from repeat topographic surveys: Improved sediment budgets. *Earth Surface Processes and Landforms*, 35, 136–156.

Williams, F., McColl, S., Fuller, I., Massey, C., Smith, H. & Neverman, A. (2021) Intersection of fluvial incision and weak geologic structures cause divergence from a universal threshold slope model of landslide occurrence. *Geomorphology*, 389, 107795. Available from: https://doi.org/10.1016/j.geomorph.2021.107795

Zhang, X., Phillips, C. & Pearce, A. (1991) Surface movement in an earthflow complex, Raukumara Peninsula, New Zealand. *Geomorphology*, 4(3–4), 261–272. Available from: https://doi.org/10.1016/0169-555X(91)90009-Y

SUPPORTING INFORMATION

Additional supporting information may be found in the online version of the article at the publisher's website.

How to cite this article: McColl, S.T., Holdsworth, C.N., Fuller, I.C., Todd, M. & Williams, F. (2022) Disproportionate and chronic sediment delivery from a fluvially controlled, deep-seated landslide in Aotearoa New Zealand. *Earth Surface Processes and Landforms*, 47(8), 1972–1988. Available from: https://doi.org/10.1002/esp.5358